Investigating the statistical error on autocorrelation for operational modal analysis

Raphaël Carpine, Silvia Ientile, Pierre Argoul

Investigating the error on autocorrelation for operational modal analysis

Raphaël Carpine[a], Silvia Ientile[a], Pierre Argoul[a]

[a] *Univ Gustave Eiffel, MAST-EMGCU, F-77454 Marne-la-Vallée, France*

Abstract

Autocorrelation is commonly used in signal processing for analyzing time signals, however the shape and magnitude of its error is rarely addressed. Previous research showed that in the general case, the error on the autocorrelation estimator of an arbitrary signal is inversely proportional to the square root of the signal length. For operational modal analysis of linear systems under unknown ambient excitation, this error seems to present a peculiar shape influencing the estimation of damping ratios. In this paper the error on autocorrelation for a linear, time-invariant system subjected to white Gaussian noise is analytically and numerically studied. It is found to be very similar to the system's response to an ambient noise, thus with a frequency content close to that of the expected autocorrelation itself. An upper bound of error magnitude is found for each mode of the system. Then, the resulting error on damping computations is investigated through numerical simulations applied to a two degrees of freedom mechanical system. Numerical outcomes show good agreement with the theoretical part and are then supported by experimental data of a prestressed concrete bridge under ambient traffic. This study allows for a better understanding and quantification of the inaccuracy on damping ratios computation through techniques using autocorrelation in time domain, notably the logarithmic decrement or time-frequency domain decomposition based on wavelet analysis.

Keywords: Autocorrelation, Linear time-invariant systems, Operational modal analysis, Ambient excitation, Damping, Wavelet analysis, Prestressed concrete bridge

1. Introduction

Techniques estimating modal structural parameters only based on the output dynamic responses became more and more popular as Operational Modal Analysis (OMA) or output-only modal analysis, particularly in the civil engineering community because they allow for the identification of the modal characteristics of a given structure under operating conditions. In ambient vibration tests, the structure under study may be subjected to several sources of excitation caused by urban traffic, seismic activity, wind, etc, which are not measured but assumed to be "broadband random" (and often modeled as a white noise), and only responses of the structure are measured. All aspects of operational modal analysis for civil engineering are covered in [1] from theoretical background to applications. OMA has become the primary modal testing method in civil engineering applications and the number of reported case studies is abundant [2, 3, 4].

A broad classification can be made for OMA methods according to two criteria: frequency domain or time domain, and Bayesian or non-Bayesian [5]. Bayesian methods were developed in time domain and frequency domain after Non-Bayesian ones. In Bayesian techniques, modal parameters are modeled as random variables with a probability distribution depending on the available information. The direct problem is first addressed: given the modal parameters, what is the distribution of data? Bayes' theorem determines the probability that an event occurs from another event already occurred, provided that these two events are interdependent. The theorem allows here to swap the roles of modal parameters and available data, so that the inverse problem: given the data, what is the distribution of the modal parameters? can also be addressed in full details. Probability is used as a measure of the relative possibility of outcomes, given a model of the system and measured data. Recently, some Bayesian methods estimating modal parameters through maximum likelihood computations were developed, allowing an estimation of their error [6, 7]. In this paper, the study is restricted to non-Bayesian methods.

As OMA is based on the assumption of a random input, non-Bayesian methods generally use certain statistical estimators with known theoretical expectations such as the correlation function or the spectral density of the mea-

sured vibrations. Common non-Bayesian methods include stochastic subspace identification (time domain) [8] and frequency domain decomposition (frequency domain), using the singular value decomposition of the power spectral density matrix [9]. In [10, 11], time–frequency instantaneous estimators are proposed for the identification of damping from signals measured in ambient vibration conditions. In [10], from each signal, a time function of modal damping and amplitude is extracted, providing punctual information on the stability and consistency of structural damping estimate. In [11], the wavelet spectral and instantaneous wavelet spectral functions defined from the continuous wavelet transform of response signals, give an estimation of modal viscous damping ratio for stationary processes and locally stationary processes. A "smoothed" estimate has been then produced, strongly depending on the choice of the time-frequency resolution of the wavelet transform. Based on energetic properties, an optimal value of this quality factor controlling the wavelet time-frequency resolution is proposed.

Numerous techniques for OMA purposes are based on autocorrelation and cross-correlation functions, especially in frequency domain using power spectrum density [12]. In this paper, only OMA methods based on the analysis of autocorrelation functions in time domain are considered, notably those that rely on the wavelet transform [13, 14] and the logarithmic decrement [15]. Estimating autocorrelation from a finite size signal inevitably introduces an error (defined as the difference with its expectation for a non-biased estimator), yet the matter of the results precision is rarely addressed, especially for the damping computations which often yield significant inaccuracies, in some cases more than 100 % [11, 16]. Bendat and Piersol [17] studied the variance of the autocorrelation estimator in the general case, and found that it is inversely proportional to the length of the acquired signal. Similarly, Vandiver [18] studied the variance of the random decrement signature, which can be directly linked to the autocorrelation function [19], and came to the same conclusion. However, to our knowledge, the special case of linear systems under white noise, and specifically the shape of the error on the associated autocorrelation, has never been investigated. The aim of this paper is to characterize the shape and magnitude of the error on the autocorrelation function estimator in time domain for responses of linear systems to unknown white Gaussian noise. The outcomes of the study allow for a better understanding and quantification of the resulting errors on modal parameters, especially damping ratios.

This paper is structured as follows: the expectation of the autocorrelation of a linear system under white Gaussian noise is reminded in section 2 and the shape and magnitude of its error is investigated in section 3. Finally, the resulting error on damping computations is derived, and numerical simulations and experimental results of a monitored bridge are presented.

2. Definitions and expected autocorrelation

For simplicity and similarity with numerical computations, we will use discrete sampled signals instead of continuous ones. In addition, the considered linear systems will have only one input and output, although they can model multiple degrees of freedom, acting as linear filters.

2.1. Reminders and notations

For discrete signals u, $v \in \mathbb{C}^{\mathbb{Z}}$, we define here the convolution product as:

$$u * v\,[n] = \Delta t \sum_{k=-\infty}^{+\infty} u[n-k]\, v[k], \tag{1}$$

where $n \in \mathbb{Z}$, and $\Delta t > 0$ is the time increment. Then autocorrelation of a finite energy signal u is defined as:

$$R_u[n] = \Delta t \sum_{k=-\infty}^{+\infty} u[k]\, u^*[k-n], \tag{2}$$

where the exponent * refers to the complex conjugate. This implies notably that $R_u[-n] = R_u^*[n]$. Alternative definitions for autocorrelation are often used, with normalization coefficients that can lead to biased or unbiased estimators [17]. We decide to use a simple definition, because it can always be normalized afterwards.

Realistically, physical signals are measured only on finite time intervals. Thus, for any discrete signal $u \in \mathbb{C}^{\mathbb{Z}}$, we introduce its windowed counterpart $\tilde{u}$:

$$\tilde{u}[n] = \begin{cases} u[n] & \text{if } n \in \{0, \ldots, N-1\} \\ 0 & \text{else,} \end{cases} \tag{3}$$

where $N \in \mathbb{N}^*$ is the number of sampled points.

2.2. Expected autocorrelation for a linear system

Let w be a discrete, white Gaussian noise, defined by:

$$w[n] \sim \mathcal{N}(0,\, \sigma^2), \tag{4}$$

where the $w[n]$ are mutually independent. Then we define the discrete response x of a linear system to w as:

$$x[n] = h * w\,[n], \tag{5}$$

where h is the discrete impulse function of the system. If $\lambda_1, \ldots, \lambda_P$ denote the poles of the system's transfer function, its impulse function can be written as [20]:

$$h[n] = \Theta[n] \sum_{p=1}^{P} A_p \mathrm{e}^{\lambda_p n \Delta t} \in \mathbb{R}, \tag{6}$$

where $A_1, \ldots, A_P$ are complex coefficients, and Θ is the discrete Heaviside function. Assuming the system is damped on each one of its modes, i.e. $\mathrm{Re}(\lambda_p) < 0$ for all p, its autocorrelation becomes:

$$\forall\, n \in \mathbb{N}, \quad R_h[n] = R_h[-n] = \sum_{p=1}^{P} B_p \mathrm{e}^{\lambda_p n \Delta t} \in \mathbb{R} \quad \text{with} \quad B_p = \Delta t \sum_{q=1}^{P} \frac{A_p A_q^*}{1 - \mathrm{e}^{(\lambda_p + \lambda_q^*)\Delta t}}. \tag{7}$$

At last, let $\tilde{x}$ be the windowed signal on interval $\{0, \ldots, N-1\}$, and $R_{\tilde{x}}$ its autocorrelation. It can be shown from Eq. (5) that:

$$\forall\, n \in \mathbb{N}, \quad \mathbb{E}\left[R_{\tilde{x}}[n]\right] = (N-n)\Delta t^2 \sigma^2 R_h[n]. \tag{8}$$

Therefore the windowed signal's autocorrelation constitutes an indirect estimator of R_h. Then, using various signal processing methods [12, 13, 14], its poles $\lambda_1, \ldots, \lambda_P$ can be computed through Eq. (7). Finally, these poles give the natural frequencies and damping ratios of the system's modes [20].

However, an error as a significant difference between autocorrelation computation and its expectation can be observed in experimental applications. This error is similar to the system's response to a random noise, i.e. oscillations at around its natural frequencies with varying amplitudes, as demonstrated in the next section.

3. Shape and magnitude of the error on autocorrelation

3.1. Autocorrelation of a windowed white Gaussian noise

To give a simple example of error on the autocorrelation of a windowed signal, and to obtain necessary preliminary results, in this part we study a windowed white Gaussian noise.

Let w be the white Gaussian noise defined by Eq. (4), and $\tilde{w}$ its windowed counterpart (see Eq. (3)). As windowed noise $\tilde{w}$ is real valued, its autocorrelation $R_{\tilde{w}}$ is even, and for $|n| \geqslant N$, $R_{\tilde{w}}[n]$ is equal to 0. Then, using Eq. (2) and $w[k]$ independence, we get:

$$\mathbb{E}\left[R_{\tilde{w}}[n]\right] = \begin{cases} N\Delta t\, \sigma^2 & \text{for } n = 0 \\ 0 & \text{for } |n| \in \{1, \ldots, N-1\}, \end{cases} \tag{9}$$

and:

$$\mathrm{Var}\left(R_{\tilde{w}}[n]\right) = \begin{cases} 2N\Delta t^2 \sigma^4 & \text{for } n = 0 \\ (N - |n|)\, \Delta t^2 \sigma^4 & \text{for } |n| \in \{1, \ldots, N-1\}. \end{cases} \tag{10}$$

Autocorrelation $R_{\tilde{w}}$ can therefore be divided into a deterministic 'spike' at $n = 0$, and a random, zero-expectation signal W:

$$R_{\tilde{w}}[n] = N\Delta t^2 \sigma^2 \delta[n] + W[n], \tag{11}$$

where $\delta[n]$ equals $1/\Delta t$ for $n = 0$, and 0 everywhere else. Variance for W is determined by Eq. (10), and as for $R_{\tilde{w}}$, it is even. In addition, for any i, j such as $0 \leqslant i < j$, $W[i]$ and $W[j]$ are uncorrelated. Simulations of $\tilde{w}$ and $R_{\tilde{w}}$ are shown in Fig. 1.

It should be noted that the 'spike' impulsion amplitude at $n = 0$, defined by Eq. (9), is proportional to N, while the standard deviation of $W[n]$, defined by Eq. (10), is proportional to $N^{1/2}$. Thus, when the number of points N increases, $R_{\tilde{w}}$ becomes closer to its expectation such as a pure 'spike'.

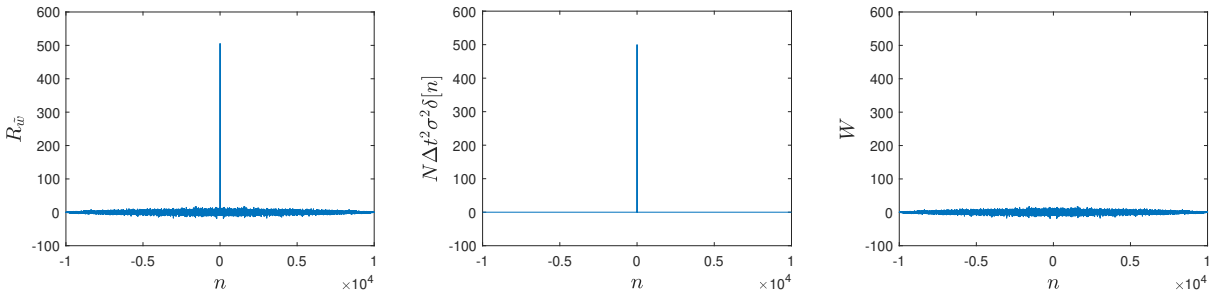

(a) (b) (c)

Figure 1: Numerical simulation of the autocorrelation $R_{\tilde{w}}$ of a windowed white Gaussian noise $\tilde{w}$ (a), its expectation $N\Delta t^2\sigma^2\delta[n]$ (b), and their difference W (c). The parameters taken are $\sigma = 1$, $\Delta t = 0.05$ and $N = 10000$.

3.2. Autocorrelation of a windowed response of a linear system to white Gaussian noise

We now study the error on autocorrelation of a windowed response of a linear system to white Gaussian noise $R_{\tilde{x}}$, i.e. the difference with its expectation. First, it is proven in Appendix A that:

$$R_{\tilde{x}}[n] \underset{N\gg n}{\approx} R_{h*\tilde{w}}[n], \tag{12}$$

with a relative error of order $1/N$. As can be seen in Fig. 2, $\tilde{x}$ and $h * \tilde{w}$ only differ around $n = 0$ and $n = N - 1$, where their difference is a free response of the system, hence the approximation. Then, using a classical formula on

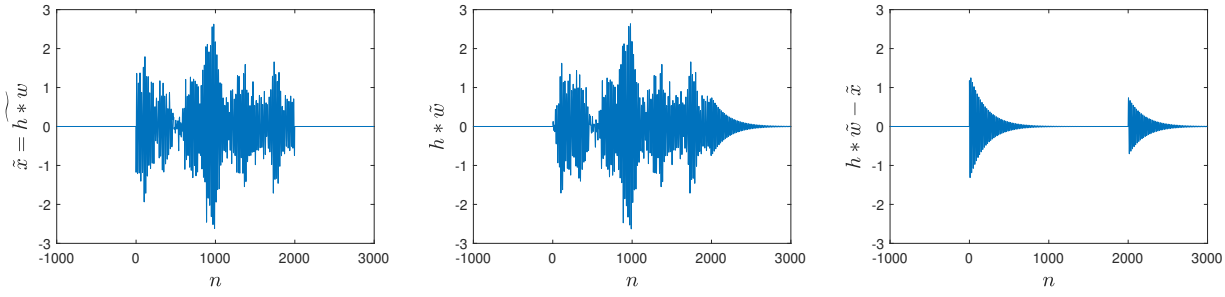

(a) (b) (c)

Figure 2: Numerical simulation of a one degree of freedom system under white Gaussian noise w, with its windowed response to w, $\tilde{x} = \widetilde{h * w}$ (a), its response $h * \tilde{w}$ to windowed noise $\tilde{w}$ (b), and their difference $h * \tilde{w} - \tilde{x}$ (c). The system's response is computed using a convolution product (see Eqs. (5) and (6)), using parameters $\lambda_1 = -0.1 + 2i\pi$, $\lambda_2 = \lambda_1^*$, $A_1 = -i$, $A_2 = A_1^*$, $\sigma = 1$, $\Delta t = 0.05$ and $N = 2000$.

autocorrelation of a convolution product [17], we get $R_{h*\tilde{w}} = R_h * R_{\tilde{w}}$, which, combined with Eq. (11), leads to:

$$R_{h*\tilde{w}}[n] = N\Delta t^2\sigma^2 R_h[n] + R_h * W\,[n]. \tag{13}$$

Autocorrelation $R_{h*\tilde{w}}$ constitutes therefore an estimation of R_h if the right-hand term $R_h * W$ remains small enough. Then it can be used to compute the system's natural frequencies and damping ratios, as stated before. This right-hand term $R_h * W$, given the shapes of R_h and W, is similar to the system's response to a random noise. Hence, as these autocorrelation signals are generally processed and filtered to isolate and analyze each mode individually, we split them into P sub-signals corresponding to each pole λ_p, by introducing $R_h^{(p)}[n] = R_h^{(p)}[-n] = B_p e^{\lambda_p n\Delta t}$ for all $n \in \mathbb{N}$, and $R_{h*\tilde{w}}^{(p)} = R_h^{(p)} * R_w$. This way, we get:

$$\mathbb{E}\left[R_{h*\tilde{w}}^{(p)}[n]\right] = N\Delta t^2\sigma^2 R_h^{(p)}[n], \tag{14}$$

and, as proven in Appendix B:

$$\mathrm{Var}\left(R_h^{(p)} * W\,[n]\right) \leqslant N\Delta t^4\sigma^4 \left|B_p\right|^2 \left[\frac{8}{1-\mathrm{e}^{(\lambda_p+\lambda_p^*)\Delta t}} + \frac{4}{\left|1-\mathrm{e}^{(\lambda_p-\lambda_p^*)\Delta t}\right|}\right] \tag{15}$$

$$\underset{|\lambda_p\Delta t|\ll 1}{\approx} N\Delta t^3\sigma^4 \left|B_p\right|^2 \left[\frac{4}{-\mathrm{Re}\left(\lambda_p\right)} + \frac{2}{\left|\mathrm{Im}\left(\lambda_p\right)\right|}\right]. \tag{16}$$

Finally, considering pole p as $\lambda_p = -\mu_p \pm \mathrm{i}\omega_{d,p}$ with μ_p as the damping constant and $\omega_{d,p}$ as the damped angular frequency, total response signal time $N\Delta t$ as T, and introducing the ratio between the characteristic amplitude of the error on pole p, $R_h^{(p)} * W$, and its expected initial amplitude $R_{h*\tilde{w}}^{(p)}[0]$, we get an upper bound α_p which satisfied:

$$\frac{\sqrt{\mathrm{Var}\left(R_h^{(p)} * W\,[n]\right)}}{\left|N\Delta t^2\sigma^2 R_h^{(p)}[0]\right|} \leqslant \alpha_p, \tag{17}$$

where:

$$\alpha_p = \sqrt{\frac{4}{\mu_p T} + \frac{2}{\omega_{d,p} T}}. \tag{18}$$

This way, an upper bound for the magnitude of the error on autocorrelation can be computed for each mode. This upper bound depends on pole λ_p of the associated mode p, predominantly its real part $-\mu_p$ for lightly damped systems (i.e. $\mu_p \ll \omega_{d,p}$). It should be noted that α_p is of order $1/N^{1/2}$, while the relative difference between $R_{\tilde{x}}$ and $R_{h*\tilde{w}}$ is of order $1/N$, thus the use of Eq. (12) is justified. The error on autocorrelation for a one degree of freedom system and its upper bound derived from Eq. (17) are presented in Fig. 3. Mode amplitude is estimated using the Continuous Wavelet Transform skeleton as described in [13], in order to better illustrate and understand the effect of the error.

Furthermore, the use of an averaging method [12], for instance dividing the signal into M sub-signals of length N/M, calculating their autocorrelation and taking the mean result, does not change the magnitude of the final error. As a matter of fact, according to the central limit theorem, and assuming the sub-signals are long enough to be considered independent, averaging the errors will reduce their magnitude by a $M^{1/2}$ coefficient, while their magnitude is inversely proportional to the square root of their size, $(N/M)^{1/2}$ (see Eq. (18)). Consequently, the square root of M will cancel out, and the resulting error will be the same as without the averaging step, making the signal total acquisition length N the only relevant parameter. This has been verified numerically, giving almost identical error profiles with and without the averaging process.

4. Applications on damping estimation

4.1. Subsequent error on damping

This error on autocorrelation eventually induces an error on the damping estimated from its exponentially decaying amplitude. To asses this error, we will consider a linear regression on the log of the amplitude of $\hat{R}_h^{(p)}$, the estimator of $R_h^{(p)}$ obtained through Eq. (8) after normalization and a filtering process (for instance, using the wavelet transform [13], singular value decomposition [15], or both [14]). For this purpose, we must first assume that the error to signal ratio (which is computed from $R_h^{(p)}$ module, $|R_h^{(p)}[n]| = |B_p\mathrm{e}^{\lambda_p n\Delta t}| = |B_p|\,\mathrm{e}^{-\mu_p n\Delta t}$, see Eqs. (7) and (17)) remains low in the autocorrelation, i.e.:

$$\alpha_p \mathrm{e}^{\mu_p n\Delta t} \ll 1. \tag{19}$$

Then, using Eq. (17), and assuming the phase shift between $\hat{R}_h^{(p)}[n]$ expectation and its error is uniformly distributed, we get:

$$\mathbb{E}\left[\ln\left|\hat{R}_h^{(p)}[n]\right|\right] \approx \ln|B_p| - \mu_p n\Delta t, \tag{20}$$

and:

$$\sqrt{\mathrm{Var}\left(\ln\left|\hat{R}_h^{(p)}[n]\right|\right)} \leqslant \sqrt{2}\,\alpha_p \mathrm{e}^{\mu_p n\Delta t}. \tag{21}$$

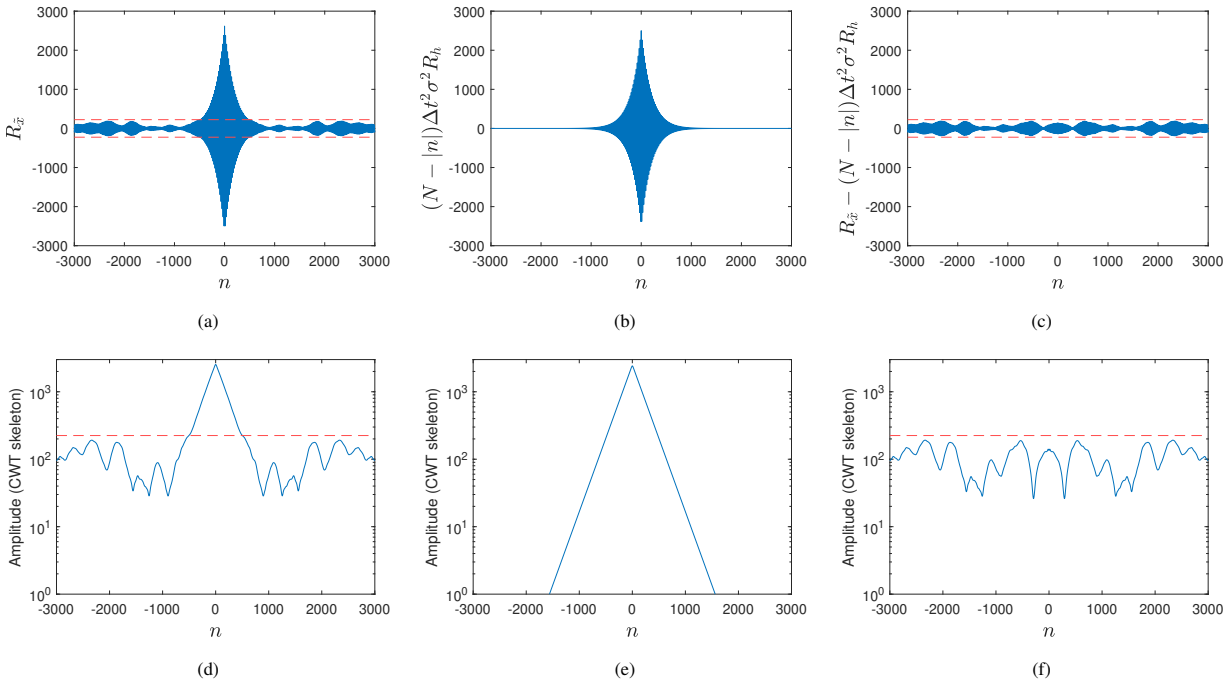

Figure 3: Numerical simulation of a one degree of freedom system under white Gaussian noise, with autocorrelation $R_{\tilde{x}}$ (a), its expectation $(N-|n|)\Delta t^2\sigma^2 R_h$ (b), and their difference, the error (c). The amplitude of $R_{\tilde{x}}$ (d), $(N-|n|)\Delta t^2\sigma^2 R_h$ (e), and their difference (f), are computed using the continuous wavelet transform skeleton [13] (log scale). Red dotted lines correspond to plus and minus the upper bound on error magnitude, derived from Eq. (17). The system's response is computed using a convolution product (see Eqs. (5) and (6)), using parameters $\lambda_1 = -0.1 + 2\mathrm{i}\pi$, $\lambda_2 = \lambda_1^*$, $A_1 = -\mathrm{i}$, $A_2 = A_1^*$, $\sigma = 1$, $\Delta t = 0.05$ and $N = 100000$ (although graphs are plotted for $|n| \leqslant 3000$ only).

Although the approximation from Eq. (20) holds up to at least the 8th order in $\alpha_p \mathrm{e}^{\mu_p n\Delta t}$, the assumption from Eq. (19) still needs to be verified. Otherwise, it would induce a bias in Eq. (20), and therefore on the estimated damping ratio. This is especially true for the end of the regression, where $\mathrm{e}^{\mu_p n\Delta t}$ is at its highest.

Then, through a linear regression on $\ln|\hat{R}_h^{(p)}|$ from $n = n_{ri}$ to $n = n_{rf}$, with a total number of points $N_r = n_{rf} - n_{ri} + 1$, the estimated damping constant $\hat{\mu}_p$ can be expressed as:

$$\hat{\mu}_p = -\boldsymbol{D}^T\boldsymbol{Y} \quad \text{where} \quad \boldsymbol{D} = \frac{6}{N_r(N_r-1)(N_r+1)\Delta t}\begin{bmatrix} -N_r+1 \\ -N_r+3 \\ \vdots \\ N_r-1 \end{bmatrix} \quad \text{and} \quad \boldsymbol{Y} = \begin{bmatrix} \ln\left|\hat{R}_h^{(p)}[n_{ri}]\right| \\ \vdots \\ \ln\left|\hat{R}_h^{(p)}[n_{rf}]\right| \end{bmatrix}, \tag{22}$$

which implies, from Eq. (20),

$$\mathbb{E}[\hat{\mu}_p] = -\boldsymbol{D}^T\mathbb{E}[\boldsymbol{Y}] \approx \mu_p, \tag{23}$$

and:

$$\sqrt{\mathrm{Var}(\hat{\mu}_p)} = \sqrt{\boldsymbol{D}^T\mathrm{Cov}(\boldsymbol{Y})\boldsymbol{D}} \leqslant \sum_{n=1}^{N_r} |D_n| \sqrt{\mathrm{Var}(Y_n)}. \tag{24}$$

We now introduce the regression initial time $t_{ri} = n_{ri}\Delta t$, final time $t_{rf} = n_{rf}\Delta t$ and total time $T_r = N_r\Delta t$. Because t_{rf} is the last moment of the regression, thus with the largest time, condition from Eq. (19) becomes $\alpha_p \mathrm{e}^{\mu_p t_{rf}} \ll 1$. Then, assuming Δt is sufficiently small ($\mu_p\Delta t \ll 1$), we get from Eqs. (21) and (24):

$$\frac{\sqrt{\mathrm{Var}(\hat{\mu}_p)}}{\mathbb{E}[\hat{\mu}_p]} \leqslant 6\sqrt{2}\,\alpha_p \mathrm{e}^{\mu_p t_{ri}} \frac{\mathrm{e}^{\mu_p T_r}(\mu_p T_r - 2) + 2\mathrm{e}^{\mu_p T_r/2}\mu_p T_r + (2\mathrm{e}^{-\mu_p T_r/2} - 1)(\mu_p T_r + 2)}{(\mu_p T_r)^3}. \tag{25}$$

Finally, this upper bound can be minimized to give the optimal value of regression time T_{opt}, which is found numerically to be equal to:

$$T_{opt} = \underset{T_r}{\operatorname{argmin}} \left(6\sqrt{2}\, \frac{e^{\mu_p T_r}(\mu_p T_r - 2) + 2e^{\mu_p T_r/2}\mu_p T_r + (2e^{-\mu_p T_r/2} - 1)(\mu_p T_r + 2)}{(\mu_p T_r)^3} \right) \simeq \frac{1.4326}{\mu_p}, \tag{26}$$

with:

$$M_{opt} = \min_{T_r} \left(6\sqrt{2}\, \frac{e^{\mu_p T_r}(\mu_p T_r - 2) + 2e^{\mu_p T_r/2}\mu_p T_r + (2e^{-\mu_p T_r/2} - 1)(\mu_p T_r + 2)}{(\mu_p T_r)^3} \right) \simeq 9.8380. \tag{27}$$

This way, we now have an optimal value of regression time T_{opt}, for which the error bound on $\hat{\mu}_p$ is minimized. Therefore, from now on, the regressions are supposed to be carried out using a total time $T_r = T_{opt}$. Considering Eq. (18), Eq. (25) becomes:

$$\frac{\sqrt{\mathrm{Var}(\hat{\mu}_p)}}{\mathbb{E}[\hat{\mu}_p]} \leqslant M_{opt} e^{\mu_p t_{ri}} \sqrt{\frac{4}{\mu_p T} + \frac{2}{\omega_{d,p} T}}. \tag{28}$$

This upper bound depends only on the mode's pole real and imaginary parts, $-\mu_p$ and $\pm\omega_{d,p}$, on the response signal total length $T = N\Delta t$, and on the regression start time t_{ri}. However, because the upper bounds found in Eqs. (15) and (24) both yield a significant margin, this upper bound may be much larger than the relative standard deviation of $\hat{\mu}_p$.

To that extent, we will study numerically and experimentally the "effective" factor M_{eff}, which replaces M_{opt} in Eq. (28) in the case of an equality, and therefore satisfies by definition the following equation:

$$M_{eff} = \frac{\sqrt{\mathrm{Var}(\hat{\mu}_p)}}{\mathbb{E}[\hat{\mu}_p]} e^{-\mu_p t_{ri}} \left(\frac{4}{\mu_p T} + \frac{2}{\omega_{d,p} T} \right)^{-1/2}. \tag{29}$$

Although M_{eff} may depend on the system parameters and regression initial and total times, we will see in the numerical and experimental applications that it seems to be a constant.

4.2. Numerical simulations

To illustrate the error on damping found in OMA, and find the effective factor M_{eff} from Eq. (29), we carry out several numerical simulations of a two degrees of freedom system pictured in Fig. 4, whose modal parameters are given in Table 1. A white Gaussian noise is applied to the mass located on the left, where the response of the system x is measured. This response is computed through a convolution product with the the system's impulse response function (see Eq. (5)). The time increment taken for the simulations is $\Delta t = 0.05$ s.

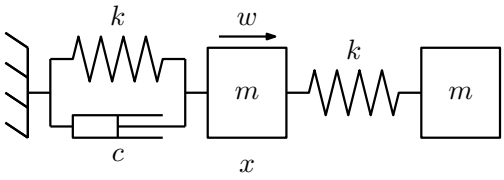

Figure 4: Numerical simulations: system modeled.

Mode p	f_p [Hz]	ζ_p [%]	$\omega_{d,p}$ [rad.s^{-1}]	μ_p [s^{-1}]	$1/\mu_p$ [s]
1	0.984	1.118	6.181	0.0691	14.5
2	2.575	1.118	16.178	0.1809	5.5

Table 1: Numerical system modal parameters.

For several response time lengths T, 100 simulations are performed. Autocorrelation of the response signals is then computed, and $\hat{R}_h$ is obtained through Eq. (8). The damping constant estimate $\hat{\mu}_p$ is computed for both modes

using a linear regression on the log of the amplitude associated with each mode, which is retrieved using the wavelet transform, as described in [13]. The regression initial time t_{ri} is set by the wavelet transform edge effect zone, and its total time T_r is set to T_{opt} to obtain minimal variance in the result, as explained earlier. System modal parameter estimates $\hat{f}_p$ and $\hat{\zeta}_p$ are then computed from the pole formula $-\hat{\mu}_p + \mathrm{i}\hat{\omega}_{d,p} = 2\pi\hat{f}_p(-\hat{\zeta}_p + \mathrm{i}(1-\hat{\zeta}_p^2)^{1/2})$ for the 100 simulations, for each response time length T and each mode, and their means and standard deviations are presented in Table 2, along with M_{eff} computed from Eq. (29). To assess the error to signal ratio in autocorrelation at the end of the regression, that is at its maximum, $\alpha_p \mathrm{e}^{\mu_p t_{rf}}$ is given for each mode (see Eq. (19)).

Response	Mode 1					Mode 2				
length T	Mean $\hat{f}_1$	Mean $\hat{\zeta}_1$	S.D. $\hat{\zeta}_1$	$\alpha_1 \mathrm{e}^{\mu_1 t_{rf}}$	M_{eff}	Mean $\hat{f}_2$	Mean $\hat{\zeta}_2$	S.D. $\hat{\zeta}_2$	$\alpha_2 \mathrm{e}^{\mu_2 t_{rf}}$	M_{eff}
[s]	[Hz]	[%]	[%]			[Hz]	[%]	[%]		
100	0.984	0.906	0.518	3.53	0.55	2.574	1.057	0.471	2.37	0.74
1000	0.984	1.065	0.223	1.12	0.79	2.576	1.127	0.157	0.75	0.88
10000	0.984	1.123	0.083	0.35	0.92	2.576	1.119	0.054	0.24	0.96
100000	0.984	1.116	0.028	0.11	1.00	2.575	1.117	0.017	0.08	0.92
1000000	0.984	1.116	0.010	0.04	1.01	2.575	1.116	0.006	0.04	0.93

Table 2: Numerical simulations: mean and standard deviation (S.D.) of damping computations from 100 simulations, for several signal lengths, with effective bound coefficient M_{eff}.

In some cases, the relative error at the end of the regression is high, i.e. $\alpha_p \mathrm{e}^{\mu_p t_{rf}} > 1$, thus the assumption from Eq. (19) is not met (both modes for $T = 100\,\mathrm{s}$, and mode 1 for $T = 1000\,\mathrm{s}$). For those cases, the mean value obtained for the damping ratio seems to be lower than expected. This indicates a bias not accounted for in Eq. (20), especially for the first mode for $T = 100\,\mathrm{s}$, where the difference with the expected value can hardly be explained by statistical chance. They also seem to give lower values for M_{eff}, which should therefore be discarded. However, in the other cases, the results for M_{eff} seem to be fairly steady across the different signal lengths (which vary by 3 orders of magnitude) and modes, with a mean value around 1. It is therefore reasonable to assume the following approximation:

$$M_{eff} \simeq 1, \tag{30}$$

which finally gives an estimate of the error on the damping computation through Eq. (29). This value, combined with Eq. (29), is a significant improvement from Eq. (28), given that M_{eff} is about ten times lesser than M_{opt}, thus providing tighter margins on the damping error estimate. To test the dependency of M_{eff} on the damping ratios, three other series of simulation were carried out using the same system with a damping factor ten times greater, ten times lesser and one hundred times lesser than first simulation's one, which all gave similar results.

These numerical results also highlight the significant inaccuracies on damping that arise from the statistical nature of OMA. For instance, estimating damping of mode 1 from a signal about 17 minutes long (corresponding to mode 1 with $T = 1000\,\mathrm{s}$ in Table 2) would result in a standard deviation of more than a fifth of its value. This corresponds to a typical situation in civil engineering, where modal parameters need to be estimated regularly at relatively short intervals, because of the temperature influence that must be evaluated afterwards.

A number of assumptions made in this study can be questioned, especially regarding the nature of excitation, namely that it is a nonstationary white Gaussian noise and that the system is linear and nonstationary as well. First, it is not in the general case a one channel signal, but rather a multi-channel signal or field, modeling the various loads on each part of the structure. Second, although the assumption of a white noise excitation is generally made in OMA [12], and can be justified under certain conditions [21], real excitation signals often present more complex profiles in frequency domain. For instance, they can be seen as white noise convoluted with a linear filter, whose poles can be extracted with those of the system and eventually discarded [22], or more generally as colored noise, whose parameters can be retrieved and taken into account in the modal analysis of the system [23]. Excitation can also be nonstationary [24], which is handled by some OMA techniques [25]. The dynamical behavior of the system itself poses other issues, as it is generally nonstationary as well, for example due to the stiffness and damping dependence of concrete on temperature for civil engineering applications, and of steel for aerospace engineering applications [26],

and can present nonlinearities for example [27] in the case of a soft impact response behavior of a reinforced concrete mock-up. For all these reasons, an application to an experimental study is presented in the next section.

4.3. Experimental testing

An experimental campaign on a bridge under ambient traffic was carried out, to support our study. The structure under study is a 74 m long bridge, supported by 6 parallel prestressed concrete beams. It is part of a series of five identical bridges build across the Marne River in France in the 1940s and 1950s under the advice of the expert engineer Eugène Freyssinet of the Campenon Bernard companies [28], as a demonstration of the capabilities of prestressed concrete for slender, long-span bridges. A total of 14 triaxial wireless accelerometers (G-Link-200) were installed on the bridge, as shown in Fig. 5. Due to the limited bandwidth of the wireless radio communication system, only the vertical acceleration signals were recorded, except for sensor 29279 (one of the mid-span accelerometers) which also monitored acceleration in the transverse direction of the bridge. Signals were sampled at 128 Hz frequency, after a numeric anti-aliasing filter with 26 Hz cutoff frequency. The signals were acquired for about 8300 s, under ambient traffic which was the main source of excitation.

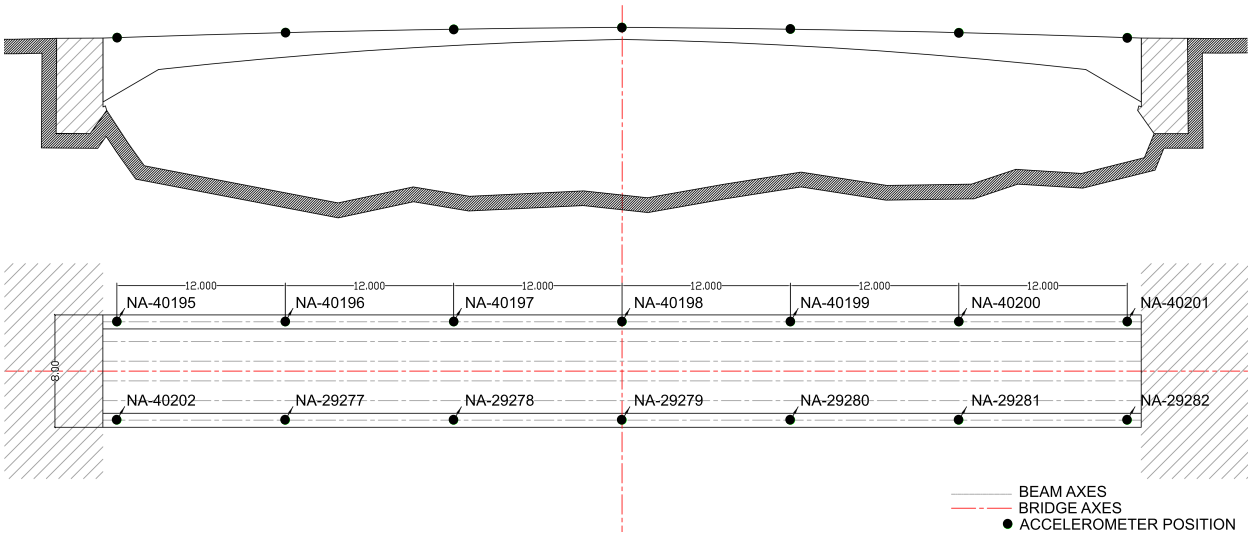

Figure 5: Experimental data: overview of the bridge accelerometric instrumentation.

To obtain the modal parameters from the accelerometric data of the bridge, the CWT-based method, described in [14], was used. This method combines cross-correlation including autocorrelation, CWT and singular value decomposition, and leads to instantaneous amplitudes, frequencies and mode shapes as functions of the cross-correlation lag. The autocorrelation function of sensor 29278 signal is showed as an example in Fig. 6a, only for positive time lags as it is even. It features an interference beat pattern, originating from the first four modes close frequencies. Fig. 6b displays the first singular value of the CWT of the cross-correlation matrix [14] between 2 Hz and 2.3 Hz, with ridges associated with the first two modes. The modal parameters are then retrieved using averages, and a linear regression on the log of the amplitude for damping. The method is slightly modified, by using T_{opt} as the total regression time, providing theoretically a minimal error on damping as explained earlier, instead of the frequency and mode shape stability stopping conditions proposed in the original paper. At first, the method is implemented on the whole signal, which provides reference parameters that will be considered the true modal parameters of the bridge for the rest of the study (hence the lack of "$\sim$" exponent for these parameters). The results obtained for the natural frequencies f_p and damping ratios ζ_p of the 10 identified modes are presented in Table 3, along with the relative error on autocorrelation at its maximum $\alpha_p e^{\mu_p t_{rf}}$, and the expected standard deviation on the ζ_p computed from Eqs. (29) and (30), which gives an estimation of their error. The corresponding mode shapes are shown in Fig. 7, where their longitudinal edges curves are smoothed using quadratic interpolation.

Observing Fig. 7's mode shapes, some modes appear to be missing, as for example the third and fourth torsional modes. This is likely due to insufficient excitation and/or excessive additive noise in their frequency range. It is not a

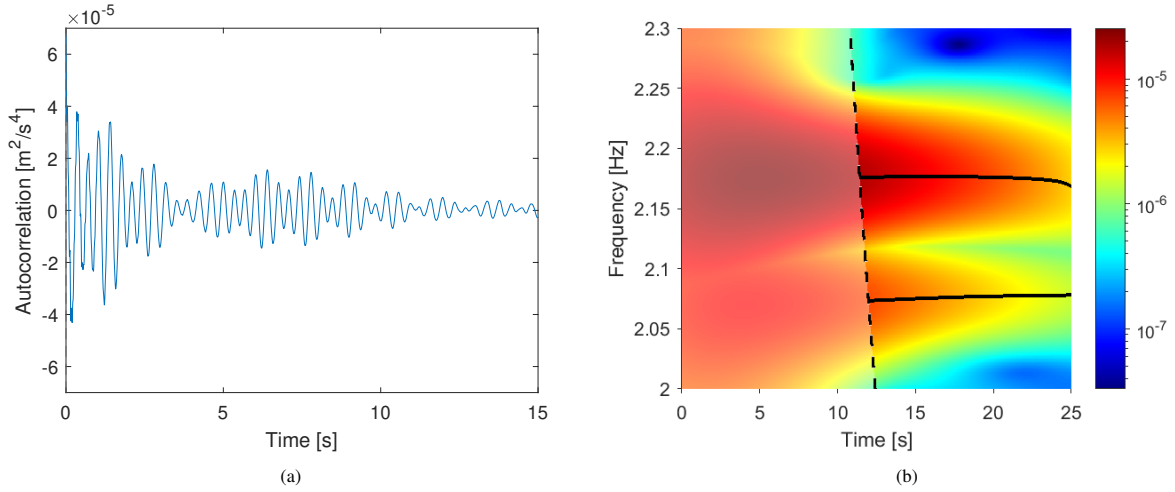

(a) (b)

Figure 6: Experimental data: (a) autocorrelation of sensor 29278 acceleration channel; (b) first singular value (module) of the CWT of the cross-correlation matrix [14] (log scale), using the Cauchy mother wavelet with quality factor $Q = 52$ whose choice of value is detailed in [29], with ridges of the first two modes. The shaded area correspond to the edge effect zone.

Mode p	f_p [Hz]	ζ_p [%]	Expected S.D. ζ_p [%]	$\alpha_p e^{\mu_p t_{rf}}$
1	2.08	0.90	0.24	1.09
2	2.18	0.94	0.25	1.14
3	2.83	0.80	0.26	1.34
4	2.94	0.95	0.46	1.95
5	5.47	1.82	0.10	0.24
6	6.51	3.70	0.37	0.42
7	7.83	4.96	0.72	0.58
8	15.04	2.36	0.17	0.30
9	16.74	1.05	0.04	0.19
10	21.13	1.04	0.05	0.19

Table 3: Experimental data: natural frequencies f_p and damping ratios ζ_p estimated from the method described in [14] using the whole signal, with expected coefficient of variation (C.V.) computed from Eqs. (29) and (30).

problem for our study however, which is not intended to be a complete modal analysis of the bridge. All the modes are pure bending or torsional modes, except for the fourth one which is a combination of torsional and lateral movement. There also seems to be spatial aliasing in the tenth mode due to a lack of sensors, which presumably corresponds to the ninth bending mode, which is why it is not displayed. Moreover, the expected standard deviation of the damping ratios and related error, is quite high as shown in Table 3. Condition from Eq. (19) is not met either for the first four modes. Therefore, although these values are taken as reference, we must keep in mind that they are potentially subject to errors.

Next, the accelerometric signals are divided into 20 sub-signals of about 415 s long in order to support the theoretical and analytical results, especially regarding M_{eff}. For each one, the same procedure from [14] is applied. The number of sub-signals is chosen from the compromise between statistical representativeness and respect of Eq. (19). Results are presented in Table 4. In this case, the assumption of Eq. (19) is not met for any mode. There are however a few modes (5, 8, 9 and 10) whose autocorrelation relative error $\alpha_p e^{\mu_p t_{rf}}$ is lower or close to 1. For these modes, the results for M_{eff} are around 1 (with a large error margin though, considering the small sample size), which supports

Mode 1
First bending mode, 2.08 Hz

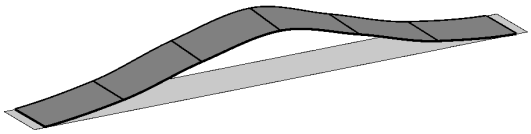

Mode 2
Second bending mode, 2.18 Hz

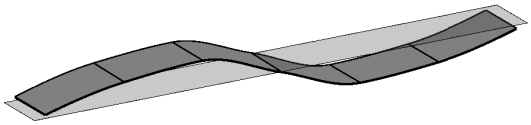

Mode 3
First torsional mode, 2.83 Hz

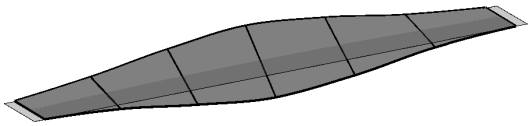

Mode 4
Mixed lateral-torsional mode, 2.94 Hz

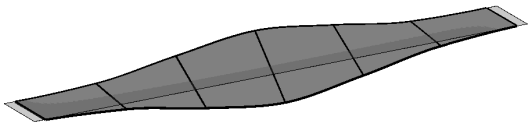

Mode 5
Second torsional mode, 5.47 Hz

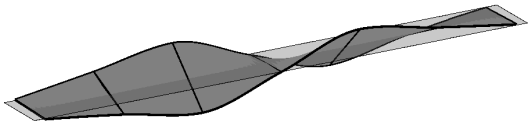

Mode 6
Third bending mode, 6.51 Hz

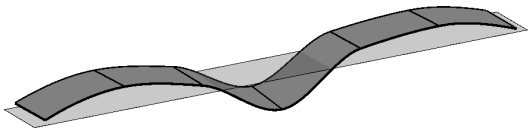

Mode 7
Fourth bending mode, 7.83 Hz

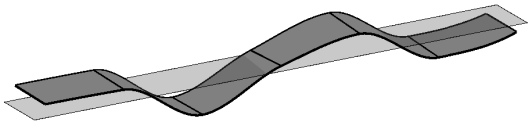

Mode 8
Fifth bending mode, 15.04 Hz

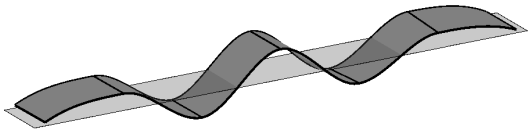

Mode 9
Fifth torsional mode, 16.74 Hz

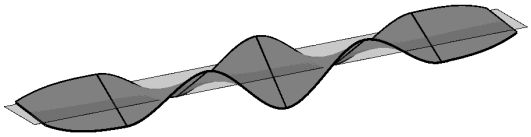

Figure 7: Experimental data: modes shapes estimated from the method described in [14] using the whole signal. The tenth mode shape could not be portrayed correctly because of a lack of sensors.

Mode p	Mean $\hat{f}_p$ [Hz]	Mean $\hat{\zeta}_p$ [%]	S.D. $\hat{\zeta}_p$ [%]	$\alpha_p e^{\mu_p t_{rf}}$	M_{eff}
1	2.07	0.56	0.25	4.90	0.24
2	2.18	0.62	0.55	5.12	0.50
3	2.84	0.54	0.43	6.00	0.37
4	2.95	0.50	0.34	8.70	0.16
5	5.45	1.43	0.62	1.06	1.37
6	6.45	2.38	0.93	1.89	0.56
7	7.99	2.76	0.67	2.60	0.21
8	15.07	1.71	0.49	1.35	0.63
9	16.76	0.86	0.25	0.84	1.25
10	21.14	0.95	0.27	0.86	1.34

Table 4: Experimental data: mean natural frequencies $\hat{f}_p$, and mean and standard deviation (S.D.) of damping ratios $\hat{\zeta}_p$ estimated from the method described in [14] using 20 sub-signals, with corresponding M_{eff}.

the numerical results of Eq. (30). Additionally, the mean values found for damping are significantly smaller than the reference values of Table 3, especially for modes with high autocorrelation relative error $\alpha_p e^{\mu_p t_{rf}}$, indicating a bias. This bias is due to the non-fulfillment of the condition from Eq. (19), as demonstrated and discussed in the numerical part.

These experimental data highlight the importance of the condition from Eq. (19), to get unbiased estimators of damping. Its non-fulfillment leads to a bias that tends to underestimate the damping ratios. This implies that one single value of damping computed from the whole length of a signal is closer to the real damping of the system than the average of several damping values computed from different parts of this signal. In addition, they show once again the large statistical errors (variance and bias) that can emerge in OMA for damping estimation, which can however be estimated using Eqs. (19), (29) and (30).

5. Conclusions

The error on autocorrelation for a discrete, finite size response of a linear system to white noise, has been shown to be very similar to its response to a random noise with varying standard deviation. This error can be divided as a sum of terms centered in the Fourier domain around the natural frequencies of the system, interfering with the meaningful signal parts of the corresponding modes which are exponentially decaying sinusoids. Thus, these error terms eventually become predominant for large enough lag values of the autocorrelation. For each mode p, the magnitude of the associated error term can be bounded by using coefficient α_p.

In this paper, the error on the derived damping ratios, resulting from the error on autocorrelation, has been investigated. An upper bound on its standard deviation, and an associated optimal regression time, have been found analytically. It indicates a relation of inverse proportionality with the square root of the response signal total length. Numerical simulations of a two degrees of freedom system corroborate the analytical results, highlighting a bias which appears when a condition on the signal length is not met. Then, a refinement of this upper bound is carried out through the numerical simulations in order to better estimate the damping computations inaccuracies. Experimental accelerometric data of a prestressed concrete single-span bridge allow for validation of the theoretical and numerical results. Indeed, the analysis on the experimental data underline the importance of the established condition on autocorrelation relative error associated with the signal length. This study shows the inaccuracies deriving from the statistical nature of the signals in operational modal analysis, which remain quite large for typical civil engineering case studies, highlighting the relevance of our work in quantifying them.

Acknowledgements

We would like to express our gratitude to the Département de Seine-et-Marne for giving us access to the bridges under their supervision, and to the Centre for Studies on Risks, the Environment, Mobility and Urban Planning, especially Anil Abdoulhoussen, Thomas Massaro and Pierre Marchand, for their fruitful help during the experimental campaign.

Appendix A. Proof of Eq. (12)

Let n be a natural integer, $n \in \mathbb{N}$. In this appendix, we will prove Eq. (12) by finding upper bounds for the expectation and variance of the difference between both terms, independent from N. This way, as the expectation of $R_{h*\tilde{w}}[n]$ is proportional to N (see Eq. (14)), the relative error is of order $1/N$. For readability, some brackets will be noted as indices from now on, for instance $w_n = w[n]$.

First, to obtain the upper bound on the expectation, Eqs. (8) and (14) are combined to find:

$$\mathbb{E}\left[R_{h*\tilde{w}}[n] - R_{\tilde{x}}[n]\right] = n\Delta t^2 \sigma^2 R_h[n].$$

Then, for the variance upper bound:

$$\tilde{x}[k] = \widetilde{h * w}\,[k] = \begin{cases} \Delta t \sum_{i=-\infty}^{+\infty} w_i h_{k-i} & \text{for } k \in \{0, \ldots, N-1\} \\ 0 & \text{else} \end{cases}$$

$$h * \tilde{w}\,[k] = \Delta t \sum_{i=0}^{N-1} w_i h_{k-i},$$

with, for all $i < 0$, $h_i = 0$. Next:

$$R_{\tilde{x}}[n] = \Delta t^3 \sum_{k=n}^{N-1} \sum_{i=-\infty}^{+\infty} w_i h_{k-i} \sum_{j=-\infty}^{+\infty} w_j h_{k-n-j} = \Delta t^3 \sum_{k=n}^{N-1} \sum_{i=-\infty}^{N-1} \sum_{j=-\infty}^{N-1} h_{k-i} h_{k-n-j} w_i w_j$$

$$R_{h*\tilde{w}}[n] = \Delta t^3 \sum_{k=-\infty}^{+\infty} \sum_{i=0}^{N-1} w_i h_{k-i} \sum_{j=0}^{N-1} w_j h_{k-n-j} = \Delta t^3 \sum_{k=n}^{+\infty} \sum_{i=0}^{N-1} \sum_{j=0}^{N-1} h_{k-i} h_{k-n-j} w_i w_j.$$

As can be seen from Eq. (6), there exist $C_0, \beta \in \mathbb{R}_+^*$ such as:

$$|h_k| \leqslant \Theta[k]\, C_0 \mathrm{e}^{-\beta k},$$

and for all $i,\ j,\ i',\ j' \in \mathbb{Z}$,

$$\mathrm{Cov}\left(w_i w_j,\ w_{i'} w_{j'}\right) = \begin{cases} 2\sigma^4 & \text{if } i = j = i' = j' \\ \sigma^4 & \text{if } i = i' \neq j = j' \text{ or } i = j' \neq j = i' \\ 0 & \text{else.} \end{cases}$$

Thus:

$$\begin{aligned}
\frac{1}{\Delta t^6}\mathrm{Var}\left(R_{h*\tilde{w}}[n]-R_{\tilde{x}}[n]\right) &= \sum_{k=n}^{N-1}\sum_{k'=n}^{N-1}\sum_{i=-\infty}^{N-1}\sum_{i'=-\infty}^{N-1}\sum_{j=-\infty}^{N-1}\sum_{j'=-\infty}^{N-1} h_{k-i}h_{k'-i'}h_{k-n-j}h_{k'-n-j'}\mathrm{Cov}\left(w_iw_j,\, w_{i'}w_{j'}\right)\\
&- 2\sum_{k=n}^{N-1}\sum_{k'=n}^{+\infty}\sum_{i=-\infty}^{N-1}\sum_{i'=0}^{N-1}\sum_{j=-\infty}^{N-1}\sum_{j'=0}^{N-1} h_{k-i}h_{k'-i'}h_{k-n-j}h_{k'-n-j'}\mathrm{Cov}\left(w_iw_j,\, w_{i'}w_{j'}\right)\\
&+ \sum_{k=n}^{+\infty}\sum_{k'=n}^{+\infty}\sum_{i=0}^{N-1}\sum_{i'=0}^{N-1}\sum_{j=0}^{N-1}\sum_{j'=0}^{N-1} h_{k-i}h_{k'-i'}h_{k-n-j}h_{k'-n-j'}\mathrm{Cov}\left(w_iw_j,\, w_{i'}w_{j'}\right)\\
&= \sigma^4\left(\sum_{k=n}^{N-1}\sum_{k'=n}^{N-1}\sum_{i=-\infty}^{N-1}\sum_{j=-\infty}^{N-1} H_{k,k',i,j} - 2\sum_{k=n}^{N-1}\sum_{k'=n}^{+\infty}\sum_{i=0}^{N-1}\sum_{j=0}^{N-1} H_{k,k',i,j} + \sum_{k=n}^{+\infty}\sum_{k'=n}^{+\infty}\sum_{i=0}^{N-1}\sum_{j=0}^{N-1} H_{k,k',i,j}\right)\\
&= \sigma^4\left(\sum_{k=n}^{N-1}\sum_{k'=n}^{N-1}\sum_{i=-\infty}^{N-1}\sum_{j=-\infty}^{-1} H_{k,k',i,j} + \sum_{k=n}^{N-1}\sum_{k'=n}^{N-1}\sum_{i=-\infty}^{-1}\sum_{j=0}^{N-1} H_{k,k',i,j} - \sum_{k=n}^{N-1}\sum_{k'=N}^{+\infty}\sum_{i=0}^{N-1}\sum_{j=0}^{N-1} H_{k,k',i,j} + \sum_{k=N}^{+\infty}\sum_{k'=n}^{+\infty}\sum_{i=0}^{N-1}\sum_{j=0}^{N-1} H_{k,k',i,j}\right)\\
&= \sigma^4\left(\sum_{k=n}^{N-1}\sum_{k'=n}^{N-1}\sum_{i=-\infty}^{-1}\sum_{j=-\infty}^{-1} H_{k,k',i,j} + \sum_{k=n}^{N-1}\sum_{k'=n}^{N-1}\sum_{i=0}^{N-1}\sum_{j=-\infty}^{-1} H_{k,k',i,j} + \sum_{k=n}^{N-1}\sum_{k'=n}^{N-1}\sum_{i=-\infty}^{-1}\sum_{j=0}^{N-1} H_{k,k',i,j} + \sum_{k=N}^{+\infty}\sum_{k'=N}^{+\infty}\sum_{i=0}^{N-1}\sum_{j=0}^{N-1} H_{k,k',i,j}\right)\\
&\leqslant 2C_0\mathrm{e}^{2\beta n}\sigma^4\left(\sum_{k=n}^{N-1}\sum_{k'=n}^{N-1}\sum_{i=-\infty}^{-1}\sum_{j=-\infty}^{-1}\mathrm{e}^{-2\beta(k+k'-i-j)} + 2\sum_{k=n}^{N-1}\sum_{k'=n}^{N-1}\sum_{i=0}^{\min(k,k')}\sum_{j=-\infty}^{-1}\mathrm{e}^{-2\beta(k+k'-i-j)} + \sum_{k=N}^{+\infty}\sum_{k'=N}^{+\infty}\sum_{i=0}^{N-1}\sum_{j=0}^{N-1}\mathrm{e}^{-2\beta(k+k'-i-j)}\right)
\end{aligned}$$

where $H_{k,k',i,j} = h_{k-i}h_{k'-i}h_{k-n-j}h_{k'-n-j} + h_{k-i}h_{k'-j}h_{k-n-j}h_{k'-n-i}$. At last:

$$\sum_{k=n}^{N-1}\sum_{k'=n}^{N-1}\sum_{i=-\infty}^{-1}\sum_{j=-\infty}^{-1}\mathrm{e}^{-2\beta(k+k'-i-j)} \leqslant \frac{\mathrm{e}^{-4\beta(n+1)}}{\left(1-\mathrm{e}^{-2\beta}\right)^4},$$

and:

$$\begin{aligned}
\sum_{k=n}^{N-1}\sum_{k'=n}^{N-1}\sum_{i=0}^{\min(k,k')}\sum_{j=-\infty}^{-1}\mathrm{e}^{-2\beta(k+k'-i-j)} &= \sum_{k=n}^{N-1}\sum_{k'=n}^{k}\sum_{i=0}^{k'}\sum_{j=-\infty}^{-1}\mathrm{e}^{-2\beta(k+k'-i-j)} + \sum_{k=n}^{N-1}\sum_{k'=k+1}^{N-1}\sum_{i=0}^{k}\sum_{j=-\infty}^{-1}\mathrm{e}^{-2\beta(k+k'-i-j)}\\
&\leqslant \frac{\mathrm{e}^{-2\beta(n+1)}}{\left(1-\mathrm{e}^{-2\beta}\right)^2}\sum_{k=0}^{+\infty}(k+1)\mathrm{e}^{-2\beta k} + \frac{\mathrm{e}^{-2\beta(n+2)}}{\left(1-\mathrm{e}^{-2\beta}\right)^4} \leqslant \frac{\mathrm{e}^{-2\beta(n+1)}\left(1+\mathrm{e}^{-2\beta}\right)}{\left(1-\mathrm{e}^{-2\beta}\right)^4},
\end{aligned}$$

and finally:

$$\sum_{k=N}^{+\infty}\sum_{k'=N}^{+\infty}\sum_{i=0}^{N-1}\sum_{j=0}^{N-1}\mathrm{e}^{-2\beta(k+k'-i-j)} \leqslant \frac{\mathrm{e}^{-4\beta}}{\left(1-\mathrm{e}^{-2\beta}\right)^4}.$$

Appendix B. Proof of Eq. (16)

First, we write $R_h^{(p)} * W$ as:

$$R_h^{(p)} * W\,[n] = \Delta t\sum_{k=-N+1}^{N-1} R_h^{(p)}[n-k]\,W_k = \Delta t\,R_h^{(p)}[n]\,W_0 + \Delta t\sum_{k=1}^{N-1}\left(R_h^{(p)}[n-k] + R_h^{(p)}[n+k]\right)W_k.$$

Then, knowing that for any $i,\ j$ such as $0 \leqslant i < j$, W_i and W_j are uncorrelated, we get:

$$\begin{aligned}
\mathrm{Var}\left(R_h^{(p)} * W[n]\right) &= \Delta t^2 \left|R_h^{(p)}[n]\right|^2 \mathrm{Var}(W_0) + \Delta t^2 \sum_{k=1}^{N-1} \left|R_h^{(p)}[n-k] + R_h^{(p)}[n+k]\right|^2 \mathrm{Var}(W_k) \\
&= \Delta t^4 \sigma^4 \left[-2N \left|R_h^{(p)}[n]\right|^2 + \sum_{k=0}^{N-1} \left|R_h^{(p)}[n-k] + R_h^{(p)}[n+k]\right|^2 (N-k)\right] \\
&\leqslant N \Delta t^4 \sigma^4 \sum_{k=0}^{+\infty} \left|R_h^{(p)}[n-k] + R_h^{(p)}[n+k]\right|^2 \\
&\leqslant N \Delta t^4 \sigma^4 \left[\sum_{k=0}^{n} \left|R_h^{(p)}[k] + R_h^{(p)}[2n-k]\right|^2 + \sum_{k=0}^{+\infty} \left|R_h^{(p)}[k] + R_h^{(p)}[2n+k]\right|^2\right] \\
&\leqslant N \Delta t^4 \sigma^4 \left|B_p\right|^2 \left[\sum_{k=0}^{n} \left|\mathrm{e}^{\lambda_p k \Delta t} + \mathrm{e}^{\lambda_p (2n-k)\Delta t}\right|^2 + \sum_{k=0}^{+\infty} \left|\mathrm{e}^{\lambda_p k \Delta t} + \mathrm{e}^{\lambda_p (2n+k)\Delta t}\right|^2\right],
\end{aligned}$$

with:

$$\sum_{k=0}^{+\infty} \left|\mathrm{e}^{\lambda_p k \Delta t} + \mathrm{e}^{\lambda_p (2n+k)\Delta t}\right|^2 = \frac{\left|1 + \mathrm{e}^{2\lambda_p n \Delta t}\right|^2}{1 - \mathrm{e}^{(\lambda_p + \lambda_p^*)\Delta t}} \leqslant \frac{4}{1 - \mathrm{e}^{(\lambda_p + \lambda_p^*)\Delta t}},$$

and finally:

$$\begin{aligned}
\sum_{k=0}^{n} \left|\mathrm{e}^{\lambda_p k \Delta t} + \mathrm{e}^{\lambda_p (2n-k)\Delta t}\right|^2 &= \frac{1 - \mathrm{e}^{(\lambda_p + \lambda_p^*)(n+1)\Delta t}}{1 - \mathrm{e}^{(\lambda_p + \lambda_p^*)\Delta t}} + \frac{1 - \mathrm{e}^{-(\lambda_p + \lambda_p^*)(n+1)\Delta t}}{1 - \mathrm{e}^{-(\lambda_p + \lambda_p^*)\Delta t}} \mathrm{e}^{2(\lambda_p + \lambda_p^*)n\Delta t} \\
&\quad + \frac{1 - \mathrm{e}^{(-\lambda_p + \lambda_p^*)(n+1)\Delta t}}{1 - \mathrm{e}^{(-\lambda_p + \lambda_p^*)\Delta t}} \mathrm{e}^{2\lambda_p n \Delta t} + \frac{1 - \mathrm{e}^{(\lambda_p - \lambda_p^*)(n+1)\Delta t}}{1 - \mathrm{e}^{(\lambda_p - \lambda_p^*)\Delta t}} \mathrm{e}^{2\lambda_p^* n \Delta t} \\
&\leqslant \frac{4}{1 - \mathrm{e}^{(\lambda_p + \lambda_p^*)\Delta t}} + \frac{4}{\left|1 - \mathrm{e}^{(\lambda_p - \lambda_p^*)\Delta t}\right|}.
\end{aligned}$$

References

[1] C. Rainieri, G. Fabbrocino, Operational modal analysis of civil engineering structures: an introduction and guide for applications, Springer, New York, 2014, oCLC: ocn871210874. doi:10.1007/978-1-4939-0767-0.

[2] P. Mohanty, D. Rixen, Operational modal analysis in the presence of harmonic excitation, Journal of Sound and Vibration 270 (1-2) (2004) 93–109. doi:10.1016/S0022-460X(03)00485-1.

[3] V. H. Vu, M. Thomas, F. Lafleur, L. Marcouiller, Towards an automatic spectral and modal identification from operational modal analysis, Journal of Sound and Vibration 332 (1) (2013) 213–227. doi:https://doi.org/10.1016/j.jsv.2012.08.019.

[4] G. Zhang, J. Ma, Z. Chen, R. Wang, Automated eigensystem realisation algorithm for operational modal analysis, Journal of Sound and Vibration 333 (15) (2014) 3550–3563. doi:10.1016/j.jsv.2014.03.024.

[5] S.-K. Au, Operational Modal Analysis, Springer Singapore, 2017. doi:10.1007/978-981-10-4118-1.

[6] K.-V. Yuen, S.-C. Kuok, Bayesian Methods for Updating Dynamic Models, Applied Mechanics Reviews 64 (1) (2011) 010802. doi:10.1115/1.4004479.

[7] B. Goller, G. Schuëller, Investigation of model uncertainties in Bayesian structural model updating, Journal of Sound and Vibration 330 (25) (2011) 6122–6136. doi:10.1016/j.jsv.2011.07.036.

[8] E. Reynders, R. Pintelon, G. De Roeck, Uncertainty bounds on modal parameters obtained from stochastic subspace identification, Mechanical Systems and Signal Processing 22 (4) (2008) 948–969, special Issue: Crack Effects in Rotordynamics. doi:https://doi.org/10.1016/j.ymssp.2007.10.009.
URL https://www.sciencedirect.com/science/article/pii/S0888327007002257

[9] R. Brincker, L. Zhang, P. Andersen, Modal identification of output-only systems using frequency domain decomposition, Smart Materials and Structures 10 (3) (2001) 441–445. doi:10.1088/0964-1726/10/3/303.

[10] R. Ceravolo, Use of instantaneous estimators for the evaluation of structural damping, Journal of Sound and Vibration 274 (1) (2004) 385–401. doi:https://doi.org/10.1016/j.jsv.2003.05.025.
URL https://www.sciencedirect.com/science/article/pii/S0022460X03011386

[11] T. Nguyen, P. Argoul, R. Ceravolo, Wavelet analysis of the structural response under ambient excitation for modal identification, in: Proc. of Eurodyn 2005, Millpress, 2005, pp. 107–112.

[12] W. Heylen, S. Lammens, P. Sas, Modal analysis theory and testing, 2nd Edition, Katholieke Univ. Leuven, Departement Werktuigkunde, Leuven, 2007.
[13] T.-P. Le, P. Paultre, Modal identification based on continuous wavelet transform and ambient excitation tests, Journal of Sound and Vibration 331 (9) (2012) 2023–2037. doi:10.1016/j.jsv.2012.01.018.
[14] T.-P. Le, P. Paultre, Modal identification based on the time–frequency domain decomposition of unknown-input dynamic tests, International Journal of Mechanical Sciences 71 (2013) 41–50. doi:10.1016/j.ijmecsci.2013.03.005.
URL https://linkinghub.elsevier.com/retrieve/pii/S0020740313000805
[15] F. Magalhães, A. Cunha, E. Caetano, R. Brincker, Damping estimation using free decays and ambient vibration tests, Mechanical Systems and Signal Processing 24 (5) (2010) 1274–1290. doi:https://doi.org/10.1016/j.ymssp.2009.02.011.
[16] R. Ceravolo, G. Abbiati, Time domain identification of structures: Comparative analysis of output-only methods, Journal of Engineering Mechanics 139 (4) (2013) 537–544. doi:10.1061/(ASCE)EM.1943-7889.0000503.
[17] J. S. Bendat, A. G. Piersol, Random data: analysis and measurement procedures, 4th Edition, Wiley series in probability and statistics, Wiley, Hoboken, N.J, 2010.
[18] J. K. Vandiver, A. B. Dunwoody, R. B. Campbell, M. F. Cook, A Mathematical Basis for the Random Decrement Vibration Signature Analysis Technique, Journal of Mechanical Design 104 (2) (1982) 307–313. doi:10.1115/1.3256341.
[19] J. Asmussen, Modal analysis based on the random decrement technique: application to civil engineering structures, Ph.D. thesis, Aalborg University (1997).
[20] M. Géradin, D. Rixen, Mechanical vibrations: theory and application to structural dynamics, third edition Edition, Wiley, Chichester, West Sussex, United Kingdom, 2015.
[21] O. Ditlevsen, Traffic loads on large bridges modeled as white-noise fields, Journal of Engineering Mechanics 120 (4) (1994) 681–694. doi:10.1061/(ASCE)0733-9399(1994)120:4(681).
[22] S. Ibrahim, J. Asmussen, R. Brincker, Modal Parameter Identification from Responses of General Unknown Random Inputs, no. 72 in Fracture and Dynamics, Dept. of Building Technology and Structural Engineering, Aalborg University, Denmark, 1995, presented at the 14th International Modal Analysis Conference, Dearborn, Michigan, USA, February 12-15, 1996 PDF for print: 12 pp.
[23] J. Cooper, M. Desforges, J. Wright, Model parameter identification using an unknown coloured random input, Mechanical Systems and Signal Processing 9 (6) (1995) 685–695. doi:10.1006/mssp.1995.0051.
[24] G. Lorenzo, C. Leon, Nonstationary and stationary noise, in: F. A. Sadjadi (Ed.), Automatic Target Recognition XVI, Vol. 6234, International Society for Optics and Photonics, SPIE, 2006, pp. 360 – 384. doi:10.1117/12.668448.
[25] L. Zhang, R. Brincker, P. Andersen, An overview of operational modal analysis: Major development and issues, Mechanical Systems and Signal Processing (2009).
[26] Y. Xia, H. Hao, G. Zanardo, A. Deeks, Long term vibration monitoring of an RC slab: Temperature and humidity effect, Engineering Structures 28 (3) (2006) 441–452. doi:10.1016/j.engstruct.2005.09.001.
[27] N. Vacca, C. Rouzaud, G. Hervé-Secourgeon, M. Galan, P. Argoul, C. Rospars, Characterization of dissipative behaviour of a reinforced concrete mock-up after soft impact tests through wavelet analysis, in: 40th IABSE Symposium Tomorrow's Megastructures, International Association for Bridge and Structural Engineering - IABSE, Nantes, France, 2018, p. 8.
[28] M. J. Chaudesaigues, La reconstruction en béton précontraint des ponts sur la Marne à Annet, Trilbardou, Esbly, Ussy et Changis-Saint-Jean, in: Annales de l'Institut technique du bâtiment et des travaux publics (in French), 1952, pp. 1–37.
[29] T.-P. Le, P. Argoul, Continuous wavelet transform for modal identification using free decay response, Journal of Sound and Vibration 277 (1) (2004) 73–100. doi:10.1016/j.jsv.2003.08.049.